EPJ Web of Conferences **227**, 01008 (2020) https://doi.org/10.1051/epjconf/202022701008
*10th European Summer School on Experimental Nuclear Astrophysics*

# Capture reaction cross-section measurements relevant to *p* process: the case of ($\alpha$, $\gamma$) reactions on $^{63}$Cu, $^{72}$Ge, $^{118}$Sn and the $^{107}$Ag($p$, $\gamma$)$^{108}$Cd reaction

*Sotirios* Harissopulos[1*], *Eleni* Vagena[1], *Michail* Axiotis[1], *Artemis* Spyrou[1**], *Georgios* Provatas[1***], *Anastasios* Lagoyannis[1], *Paraskevi* Dimitriou[1], and *Hans Werner* Becker[2]

[1]Inst. of Nuclear and Particle Physics, NCSR "Demokritos", 153.10 Aghia Paraskevi, Athens, Greece
[2]DTL/RUBION, Ruhr-Universität, Universitätsstrasse 150, 40781 Bochum, Germany

**Abstract.** The cross sections of the $^{72}$Ge$(\alpha,\gamma)^{76}$Se and $^{107}$Ag$(p,\gamma)^{108}$Cd reactions were measured at energies relevant to *p*-process nucleosynthesis. The new data, together with cross section results from our previous $(\alpha,\gamma)$ measurements on $^{65}$Cu and $^{118}$Sn and other $(\alpha,\gamma)$ cross-section data reported in literature are compared with statistical model calculations performed using the latest version (1.9) of the statistical model code TALYS. In addition, the effect on these calculations of different combinations of the optical model potentials (OMPs), nuclear level densities (NLDs) and $\gamma$-ray strength functions ($\gamma$SFs) entering the calculations was investigated.

## 1 Introduction

The Hauser-Feshbach (HF) theory is extensively used to calculate the reaction cross sections required to solve the *p*-process reaction network [1, 2]. HF calculations require as input parameters nuclear masses, Nuclear Level Densities (NLDs) and transmission coefficients, with the later ones obtained from nucleon-nucleus and $\alpha$-particle–nucleus Optical Model Potentials (OMPs) and $\gamma$-ray strength functions ($\gamma$SFs). As these nuclear parameters are described by either phenomenological or microscopic models, nuclear physics uncertainties entering *p*-nuclei abundance calculations depend strongly on their reliability that has to be checked. This check is the main motivation of all experimental works, including the present one, aiming at determining cross sections of capture reactions relevant to the *p* process. Their comparison with HF calculations allows to evaluate and, furthermore, improve the OMP, NLD and $\gamma$SF models.

## 2 Cross section measurements

In this work, we report on the reactions listed in table 1. The corresponding beam energy range covered, enrichment and target's areal density ("thicknesses") $\xi$ are also given in this table. The enrichments were provided by the isotope manufacturers, whereas the target thicknesses were determined using the Rutherford Backscattering Method (RBS) [3]. In the case

*e-mail: sharisop@inp.demokritos.gr
**Current address: NCSL, Michigan State University, East Lansing, MI 48824, USA
***Current address: Ruđer Bošković Institute, Bijenička cesta 54, 10000 Zagreb, Croatia

of the $^{107}$Ag$(p,\gamma)^{108}$Cd reaction, a natural target was used and the corresponding $\xi$ listed in table 1 refers to the $^{107}$Ag target isotope. The beam energy losses $\Delta E$ in the targets given in this table were calculated at the corresponding lowest beam energy using the code SRIM [4].

**Table 1.** Nuclear reactions, energy ranges and relevant target properties (see text in sect. 2 for details)

| Reaction | Energy range (MeV) | Areal density $\xi$ ($\mu$g/cm$^2$) | Enrichment (%) | $\Delta$E (keV) |
|---|---|---|---|---|
| $^{65}$Cu$(\alpha,\gamma)^{69}$Ga | 5.2 – 8.1 | 162±10 | 99.7 | 66 |
| $^{72}$Ge$(\alpha,\gamma)^{76}$Se | 5.7 – 10.5 | 590±90 | 98.2 | 225 |
| $^{118}$Sn$(\alpha,\gamma)^{122}$Te | 10.5 –11.7 | 1700±150 | 98 | 362 |
| $^{107}$Ag$(p,\gamma)^{108}$Cd | 2.1 – 4 | 420±25 | 51.839 | 27 |

The $(\alpha,\gamma)$ cross sections reported in this work were measured with the $4\pi$ $\gamma$-summing technique that is described in detail in Refs. [2, 5–8] and is, therefore, not presented here. The cross sections of the $^{107}$Ag$(p,\gamma)^{108}$Cd reaction were determined by measuring $\gamma$-angular distributions at seven proton beam energies using three hyper-pure germanium (HPGe) detectors with relative efficiencies of almost 100%. For this purpose, $\gamma$-singles spectra were measured at every beam energy at six different angles (0°, 25°, 55°, 65°, 80°, 90°) with respect to the beam direction. Details on the method applied to obtain cross sections from $\gamma$-angular distribution measurements can be found in [2, 9–11]. Both techniques are summarized and compared in [2]. Typical spectra for the $(\alpha,\gamma)$ reactions on $^{65}$Cu and $^{118}$Sn have already presented in Refs. [12, 13] and [14, 15], respectively. The corresponding measurements were re-analyzed and the cross sections reported in the present work were derived. For the $^{72}$Ge$(\alpha,\gamma)^{76}$Se and $^{107}$Ag$(p,\gamma)^{108}$Cd reactions, $\gamma$-singles spectra are plotted in figure 1.

The spectra shown in figure 1 for $^{72}$Ge$(\alpha,\gamma)^{76}$Se were measured at $\alpha$-beam energies of 10, 9 and 8 MeV. Panel (a) depicts the high-energy part of these spectra, where the corresponding sum-peaks labeled with $\gamma_{\Sigma,0}$ appear. These peaks result from the summing of all $\gamma$ cascades populating the ground state of the produced $^{76}$Se compound nucleus (see, e.g., in [2] for more details). At 10 MeV, the $\gamma_{\Sigma,0}$ peak is located at 14.406 MeV. The arrows indicate the position of the corresponding single escape peak ("-0.511") and that of a second peak at 13.284 MeV. The presence of the latter peak in the spectra is expected: its energy difference from $\gamma_{\Sigma,0}$ is 1.1211 MeV, which is the energy of the $0_2^+$ level of $^{76}$Se. This level decays to the first excited $2_1^+$ state via an $E2$ $\gamma$ transition and to the ground $0_1^+$ state by means of an

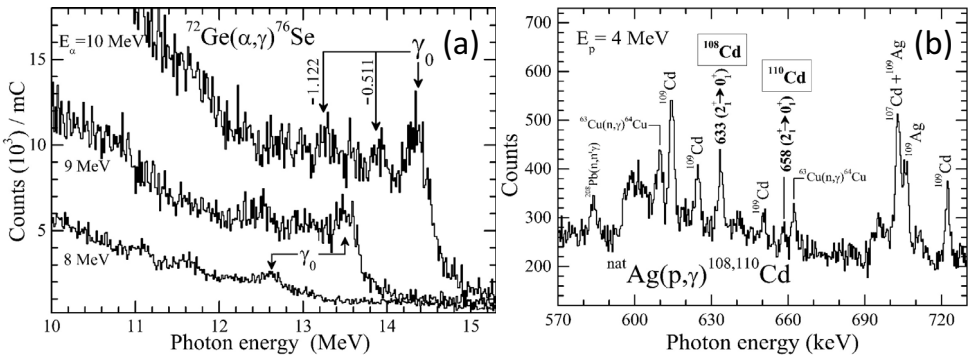


**Figure 1.** Typical $\gamma$-singles spectra measured in the present work for $^{72}$Ge$(\alpha,\gamma)^{76}$Se (left) and $^{107}$Ag$(p,\gamma)^{108}$Cd (right). For details see in the text of section 2.

$E0$ transition. As a result, a second sum peak can be formed, due to $\gamma$ cascades populating the $0_2^+$ state. Its intensity is expected proportional to that of the $E0$ transition. Following the data analysis procedure described in detail in [2], the cross sections of the $^{72}$Ge$(\alpha,\gamma)^{76}$Se reaction were determined from the absolute intensity of these two sum peaks.

The $\gamma$ spectrum plotted in figure 1 for the $^{107}$Ag$(p,\gamma)^{108}$Cd reaction was measured at a proton beam energy of 4 MeV with a HPGe detector positioned at an angle of zero degrees. Panel (b) focuses on the energy region around the 633-keV peak that belongs to the $2_1^+ \rightarrow 0_1^+$ $\gamma$-transition of $^{108}$Cd. It is worth noting that allmost all other stong peaks present in panel (b) stemm either from $(p,n)$ reactions on $^{107}$Ag and $^{109}$Ag or from $(p,p\gamma\prime)$ reactions on these target isotopes. The cross section of the $^{107}$Ag$(p,\gamma)^{108}$Cd reaction was obtained from the absolute $\gamma$-angular distributions of the 633-keV $\gamma$ ray, which did not show a signifficant angle dependence. Hence, the absolute $A_0$ coefficients of the measured $\gamma$-angular distributions, which are necessary to extract the cross section, were obtained from the average value of the data points of the corresponding $\gamma$-angular distributions (see in [11] for details).

It is worth emphasizing that primary $\gamma$ rays deexciting the entry state of the produced compound nucleus $^{108}$Cd were hardly visible in the spectra, although the possible spin values of this state are in favor of these $\gamma$ rays and especially the one directly to the ground state, often refered to as $\gamma_0$. (see in [2] for details). Due to counting statistics, we cannot à *priori* rule out the existence of $\gamma_0$ with a weak intensity. In addition to the 633-keV $2_1^+ \rightarrow 0_1^+$ transition, the ground state is populated by a 1602 keV $\gamma$ transition deexciting the $2_2^+$ level. The latter transition is not clearly visible in the spectra. However, according to existing nuclear stracture data [16], it has an almost equal intensity with that of the $2_2^+ \rightarrow 2_1^+$ 969-keV $\gamma$ ray, which clearly appears in the spectra measured at the higher beam energies. In addition, part of the intensity of the $\gamma$ transitions feeding the $0_3^+$ state at 1913.4 keV must be taken into account as this state is deexcited with two $E2$ $\gamma$ rays as well as via a $E0$ transition. Under these conditions, it is mandatory to add the intensities of all aforementioned weak or "missing" transitions to the intensity of the 633-keV $\gamma$ transition, Based on our experience gained by studying $(p,\gamma)$ reactions on nuclei with similar excitation spectra in the same mass region, we estimated that the extra intensity to be added amounts to at least 10% to that of the 633-keV $\gamma$ transition. Hence, the absolute intensity of the latter transition was increased by 10% to derive the total cross section.

## 3 Experimental cross sections and TALYS calculations

Our experimental cross-section data are given in tables 2 and 3 for the $(\alpha,\gamma)$ reactions and for $^{107}$Ag$(p,\gamma)^{108}$Cd, respectively. The former ones are compared with the theoretical predictions of the Hauser-Feshbach (HF) theory in Fig. 2. In this figure, we also compare HF calculations with the cross sections of the $^{63}$Cu$(\alpha,\gamma)^{67}$Ga, $^{70}$Ge$(\alpha,\gamma)^{74}$Se and $^{74}$Ge$(\alpha,\gamma)^{78}$Se reactions reported in [18], [19] and [20], respectively. A comparison of the cross sections of $^{107}$Ag$(p,\gamma)^{108}$Cd with HF calculations is shown in Fig. 3. The experimental data, shown in both figures with solid circles, have been corrected for electron screening effects. These, together with the relevant correction procedure, are discussed in [11].The HF calculations were performed with the latest version (1.9) of the statistical model code TALYS [17].

TALYS 1.9 offers several OMP, NLD, and $\gamma$SF models as input options. As a result, cross section calculations can be performed with 768 combinations of OMPs, NLDs, and $\gamma$SFs. The different models for these nuclear parameters are summarized in table 8 of Ref. [6]. In the case of the $(\alpha,\gamma)$ reactions reported in the present work we focused on specific model combinations of nucleon–nucleus OMPs, $\alpha$–particle OMPs ($\alpha$OMPs), Nuclear Level Densities (NLD) and $\gamma$-ray strength functions ($\gamma$SF), which are labeled TALYS-1, TALYS-2, TALYS-3, TALYS-4 and TALYS-default. The $(\alpha,\gamma)$ cross sections calculated using these

**Table 2.** Screening corrected total cross sections ($\sigma_{\rm T}$) measured for $^{65}$Cu$(\alpha,\gamma)^{69}$Ga, $^{72}$Ge$(\alpha,\gamma)^{76}$Se and $^{118}$Sn$(\alpha,\gamma)^{122}$Te at center-of-mass energies $E_{c.m.}$. $f_s$ are the screening correction factors.

| $^{65}$Cu$(\alpha,\gamma)^{69}$Ga | | | $^{72}$Ge$(\alpha,\gamma)^{76}$Se | | | $^{118}$Sn$(\alpha,\gamma)^{122}$Te | | |
|---|---|---|---|---|---|---|---|---|
| $E_{c.m.}$ $(MeV)$ | $f_s$ | $\sigma_{\rm T}$ $(\mu b)$ | $E_{c.m.}$ $(MeV)$ | $f_s$ | $\sigma_{\rm T}$ $(\mu b)$ | $E_{c.m.}$ $(MeV)$ | $f_s$ | $\sigma_{\rm T}$ $(\mu b)$ |
| 4.867 | 1.094 | $1.9 \pm 0.6$ | 5.294 | 1.116 | $0.8 \pm 0.25$ | 9.980 | 1.097 | $3.8 \pm 1.4$ |
| 5.056 | 1.089 | $4.2 \pm 1.1$ | 5.485 | 1.110 | $1.7 \pm 0.5$ | 10.176 | 1.094 | $7 \pm 2$ |
| 5.245 | 1.084 | $10.1 \pm 2.3$ | 5.677 | 1.104 | $5.1 \pm 1.4$ | 10.371 | 1.091 | $8.5 \pm 2.2$ |
| 5.434 | 1.080 | $19.5 \pm 3.6$ | 5.868 | 1.099 | $7.6 \pm 2.1$ | 10.567 | 1.089 | $12.5 \pm 3.2$ |
| 5.623 | 1.075 | $38 \pm 7$ | 6.060 | 1.094 | $11.7 \pm 3.1$ | 10.762 | 1.086 | $17.2 \pm 3.9$ |
| 5.812 | 1.072 | $70 \pm 12$ | 6.537 | 1.083 | $7.4 \pm 2$ | 10.957 | 1.084 | $22.5 \pm 4.9$ |
| 6.190 | 1.065 | $85 \pm 12$ | 7.013 | 1.075 | $10.5 \pm 2.8$ | 11.152 | 1.082 | $44.1 \pm 9.5$ |
| 6.567 | 1.059 | $76 \pm 11$ | 7.490 | 1.067 | $12.2 \pm 3.4$ | | | |
| 7.606 | 1.047 | $106 \pm 16$ | 7.968 | 1.061 | $31.7 \pm 8.5$ | | | |
| | | | 8.444 | 1.056 | $48 \pm 13$ | | | |
| | | | 8.921 | 1.051 | $78 \pm 21$ | | | |
| | | | 9.397 | 1.047 | $127 \pm 34$ | | | |
| | | | 9.873 | 1.044 | $106 \pm 28$ | | | |

**Table 3.** Same as in table 2, but for the total cross sections $\sigma_{\rm T}$ measured for $^{107}$Ag$(p,\gamma)^{108}$Cd.

| $E_{c.m.}$ $(MeV)$ | $f_s$ | $\sigma_{\rm T}$ $(\mu b)$ |
|---|---|---|
| 2.067 | 1.117 | $2.2 \pm 0.7$ |
| 2.166 | 1.108 | $3.1 \pm 0.5$ |
| 2.313 | 1.098 | $4.4 \pm 0.4$ |
| 2.462 | 1.088 | $7.3 \pm 0.7$ |
| 2.710 | 1.076 | $9.7 \pm 0.9$ |
| 2.959 | 1.066 | $17.9 \pm 1.6$ |
| 3.455 | 1.052 | $44.5 \pm 3.6$ |
| 3.951 | 1.043 | $149 \pm 15$ |

combinations are plotted in Fig. 2 as dashed, dotted, dash-dotted, dash-dotted-dotted and solid black curves. The first three combinations are explained in [11]. TALYS-4 refers to the combination of [21] for the nucleon-nucleus OMP, the dispersive model (OMP-III) of [22] for the $\alpha$OMP, the temperature-dependent Hartree-Fock-Bogolyubov model of [23] for NLD, and the $\gamma$SF model of [24]. TALYS-default is the standard combination of TALYS 1.9 in which the nucleon-nucleus OMP of [25], the $\alpha$OMP of [26], the TALYS-specific NLDs [17] and the $\gamma$SF of [27] are combined.

The selected combinations aim at demostrating the different results obtained using exclusively phenomenological or solely semi-microscopic combinations of the nuclear parameters entering the HF calculations. In the former category belong TALYS-default and TALYS-1, which differ only in the $\alpha$OMP used, i.e. that of [26] and the TALYS-specific one [17], respectively. The comparison of the corresponding solid and dashed curves at beam energies below the opening of the $(\alpha, n)$ channel, indicates that using the latter $\alpha$OMP results in cross sections that can be up to one order of magnitude larger than those obtained with the former one. In the second category of semi-microscopic TALYS combinations, i.e. TALYS-2, TALYS-3 and TALYS-4, the $\alpha$OMP used is the semi-microscopic $\alpha$OMP model of [22].

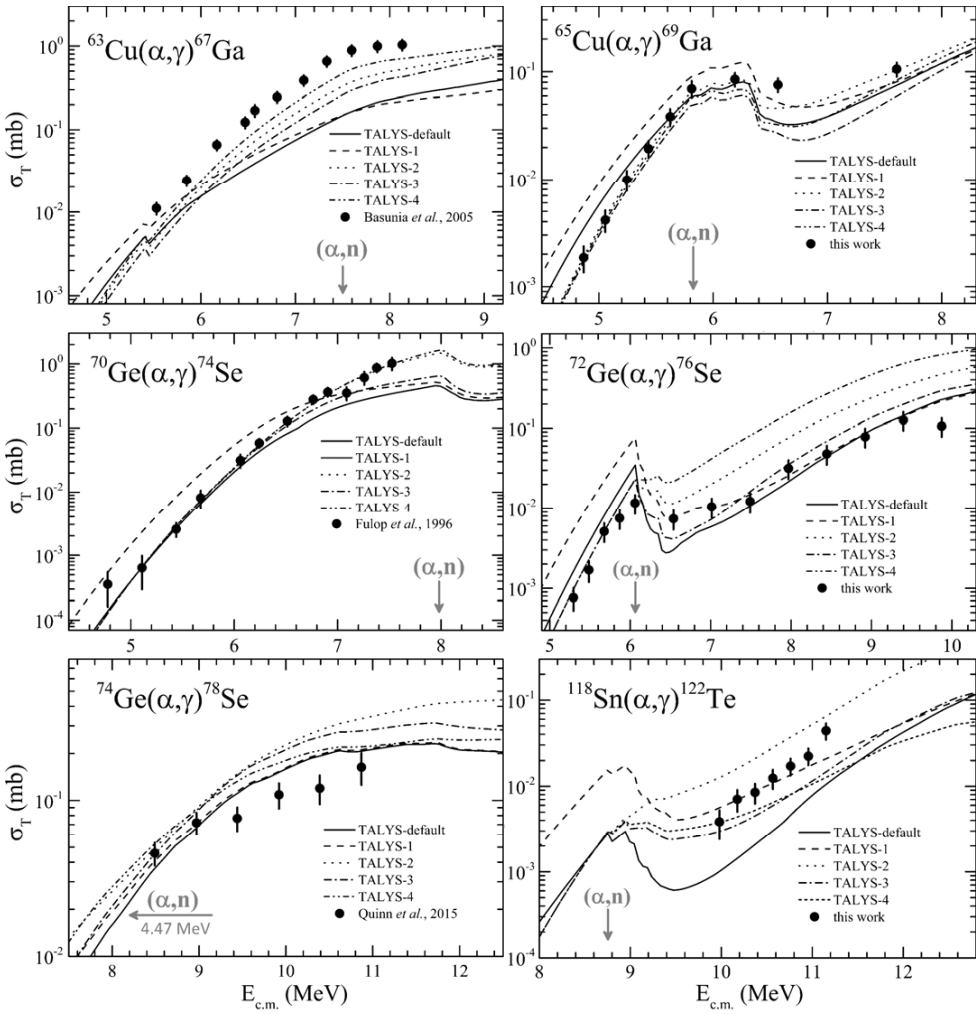


**Figure 2.** Comparison of experimental $(\alpha, \gamma)$ cross sections (black solid circles) with TALYS calculations. Details are given in section 3.

According to Fig. 2, the use of the latter $\alpha$OMP in HF calculations delivers -on the average- cross sections smaller than those derived with the phenomenological $\alpha$OMP of [26]. In addition, at energies below the $(\alpha, n)$ threshold that is indicated in Fig. 2 with a grey arrow, the TALYS-2, TALYS-3 and TALYS-4 semi-microscopic calculations are in better agreement with the experimental ones compared to those of TALYS-default. Notably, these three semi-microscopic combinations use the semi-microscopic $\alpha$OMP of [22]. It is worth noting that at energies above the opening the $(\alpha, n)$ channel, the HF calculations depend not only on the $\alpha$OMP but also to the other nuclear parameters (NLDs, $\gamma$SFs) entering the calculations. Therefore any comparison regarding the predictive power of the different $\alpha$OMPs should be limited to energies below the $(\alpha, n)$ threshold. Under these conditions, the data measured for $^{74}$Ge$(\alpha, \gamma)^{78}$Se and $^{118}$Sn$(\alpha, \gamma)^{122}$Te are not suitable to draw any conclusion on the predictive power of different $\alpha$OMP models. These considerations apply also in the case of the $^{107}$Ag$(p, \gamma)^{108}$Cd reaction for the proton OMPs.

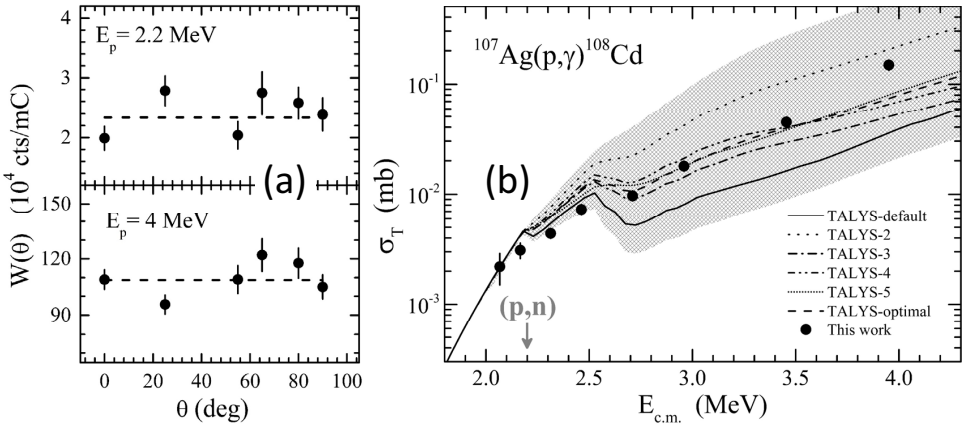


**Figure 3.** Panel (a): Typical angular distributions of the 633-keV $2_1^+ \rightarrow 0_1^+$ transition of $^{108}$Cd obtained at the lowest (2.2 MeV) and highest (4 MeV) proton beam energies measured. The dashed curves indicate the average value of the data points, which was used to derive the cross section at the corresponing beam energies as descussed in [11]. Panel (b): Comparison of the experimental cross sections (black solid circles) of the $^{107}$Ag$(p,\gamma)^{108}$Cd reaction with TALYS calculations. Details are given in section 3.

Apart from the aforementioned TALYS combinations, we adopted two additional combinations to compare the experimental cross sections of the $^{107}$Ag$(p,\gamma)^{108}$Cd reaction with HF calculations. These are shown in Fig. 3 as shorted-dotted and dashed curves. The former refers to TALYS-5, which is a semi-microscopic combination as well, whereas the latter one does not now correspond to the previous phenomenological TALYS-1 but to a arbitrary combination of input parameters resulting from a $\chi^2$ analysis, i.e. it corresponds to the combination that reproduces experimental data the best. As such we labeled it as TALYS-optimal. TALYS-5 combines the nucleon-nucleus OMP of [28], the $\alpha$OMP of [22], the NLDs of [29] and the $\gamma$SF of [30]. In the case of these data, TALYS-optimal is a combination of two phenomenological models, i.e. the nucleon-nucleus OMP of [25] and the $\alpha$OMP of [31] with the semi-microscopic models of NLDs of [29] and the $\gamma$SF of [32].

According to figure 3, up to the opening of the $(\alpha, n)$ channel indicated by the vertical grey arrow, the HF calculations agree well with the data. Moreover, the phenomenological and the semi-microscopic predictions are almost identical. At higher energies, the cross sections resulting from the different TALYS combinations start to deviate signifficantly and the data are reproduced the best by the TALYS-optimal combination, However, the curve corresponding to the pure semi-microscopic combination of TALYS-5 can hardly be distinguished from the one resulting from best "fit" to data, i.e. the TALYS-optimal combination. Finally, for the $^{107}$Ag$(p,\gamma)^{108}$Cd reaction, we have used all 768 possible combinations of the models available in TALYS 1.9 to obtain 768 cross section excitation function curves that span a range depicted by the shaded areas in Fig. 3. Obviously, this shaded area can be interpreted as the range of the uncertainties in the cross section calculations associated with the different models that were used by TALYS.

We acknowledge support of this work by the project "CALIBRA/EYIE" (MIS 5002799), which is implemented under the Action "Reinforcement of the Research and Innovation Infrastructures", funded by the Operational Programme "Competitiveness, Entrepreneurship and Innovation" (NSRF 2014-2020) and co-financed by Greece and the European Union (European Regional Development Fund).

## References

[1] M. Arnould and S. Goriely, Phys. Rep. **384**, 1 (2003).
[2] Sotirios V. Harissopulos, Eur. Phys. J. Plus **133**, 332 (2018).
[3] Yongqiang Wang, Michael Nastasi, *Handbook of Modern Ion Beam Materials Analysis* (Materials Research Society, Cambridge University Press, Cambridge, 2010).
[4] J.F. Ziegler, J.P. Biersack, Code SRIM Version 2008 (available online at http://srim.org). Full description given by J.F. Ziegler, J.P. Biersack, U. Littmark, *The Stopping and Range of Ions in Solids* (Pergamon, New York, 1985).
[5] S. Harissopulos *et al.*, Phys. Rev. C **87**, 025806 (2013).
[6] V. Foteinou *et al.*, Eur. Phys. J. A **55**, 67 (2019).
[7] A. Spyrou *et al.*, Phys. Rev. C **76**, 015802 (2007).
[8] A. Spyrou *et al.*, Phys. Rev. C **77**, 065801 (2008).
[9] S. Galanopoulos *et al.*, Phys. Rev. C **67**, 015801 (2003).
[10] S. Harissopulos *et al.*, Phys. Rev. C **93**, 025804 (2016).
[11] V. Foteinou *et al.*, Phys. Rev. C **97**, 035805 (2018).
[12] A. Lagoyannis *et al.*, *Proceeedings, 2nd lntemational Conference on Frontiers in Nuclear Structure, Astrophysics, and Reactions – FINUSTAR2, Crete, Greece, 10–14 September 2007*, edited by P. Demetriou, R. Julin, and S. V. Harissopulos (AIP Conference Proceedings, New York, Vol. 1012, 2008), p. 179.
[13] P. Demetriou *et al.*, *Proceeedings, 13th International Symposium on Capture Gamma-Ray Spectroscopy and Related Topics – CGS 13, Cologne, Germany, 25–29 August 2008*, edited by J. Jolie, A. Zilges, N. Warr, and A. Blazhev (AIP Conference Proceedings, New York, Vol. 1090, 2009), p. 293.
[14] S. Harissopulos *et al.*, J. Phys. G: Nucl. Part. Phys. **31**, S1417 (2005).
[15] S. Harissopulos *et al.*, Nucl. Phys. A **758**, 505c (2005).
[16] IAEA Live Chart of Nuclides, *Nuclear Structure and Decay Data based on the Evaluated Nuclear Structure Data File (ENSDF)*; http://www-nds.iaea.org/livechart/.
[17] Nuclear-reaction code TALYS Version 1.9 (available at http://www.talys.eu/home).
[18] M. S. Basunia *et al.*, Phys. Rev. C **71**, 035801 (2005).
[19] Zs. Fülöp *et al.*, Z. Phys A **355**, 203 (1996).
[20] S. J. Quinn *et al.*, Phys. Rev. C **92**, 045805 (2015).
[21] E. Bauge *et al.*, Phys. Rev C **63**, 024607 (2001).
[22] P. Demetriou *et al.*, Nucl. Phys. A **707**, 253 (2002).
[23] S. Hillaire *et al.*, Phys. Rev. C **86**, 064319 (2012).
[24] S. Goriely *at al.*, Nucl. Phys. A **739**, 331 (2004).
[25] A.J. Koning and J.P. Delaroche, Nucl. Phys. A **713**, 231 (2003).
[26] V. Avrigeanu *et al.*, Phys. Rev. C **90**, 044612 (2014).
[27] J. Kopecky and M. Uhl, Phys. Rev. C **41**, 1941 (1990).
[28] E. Bauge, J.P. Delaroche, M. Girod, Phys. Rev. C **63**, 024607 (2001).
[29] S. Goriely, S. Hilaire, A.J. Koning, Phys. Rev. C **78**, 064307 (2008).
[30] M. Martini *et al.*, Phys. Rev. C **94**, 014304 (2016).
[31] M. Nolte, H. Machner, J. Bojowald, Phys. Rev. C **36**, 1312 (1987).
[32] I. Daoutidis, S. Goriely, Phys. Rev. C **86**, 034328 (2012).